Stabilization of Insulin as a Therapeutic Protein Assembly via Enhanced Aromatic-Aromatic Interactions

Nischay K. Rege, Nalinda P. Wickramasinghe, Alisar N. Tustan, Nelson B. Phillips, Vivien C. Yee, Faramarz Ismail-Beigi, & Michael A. Weiss

Purpose of Supplement

We provide 12 Supplemental Figures and 12 Supplemental Tables as cited in the main text. The information pertains to five aspects: (i) tabulation of *ab initio* and molecular mechanics calculations; (ii) details of the crystal structure of Trp^{B26}, Orn^{B29}-insulin, corresponding NMR studies, and comparison with WT insulin; (iii) additional control SEC studies; (iv) additional rat studies; and (iv) details regarding the structural properties of insulin as exploited in protein engineering. The figures and tables are as follows

Table of Contents

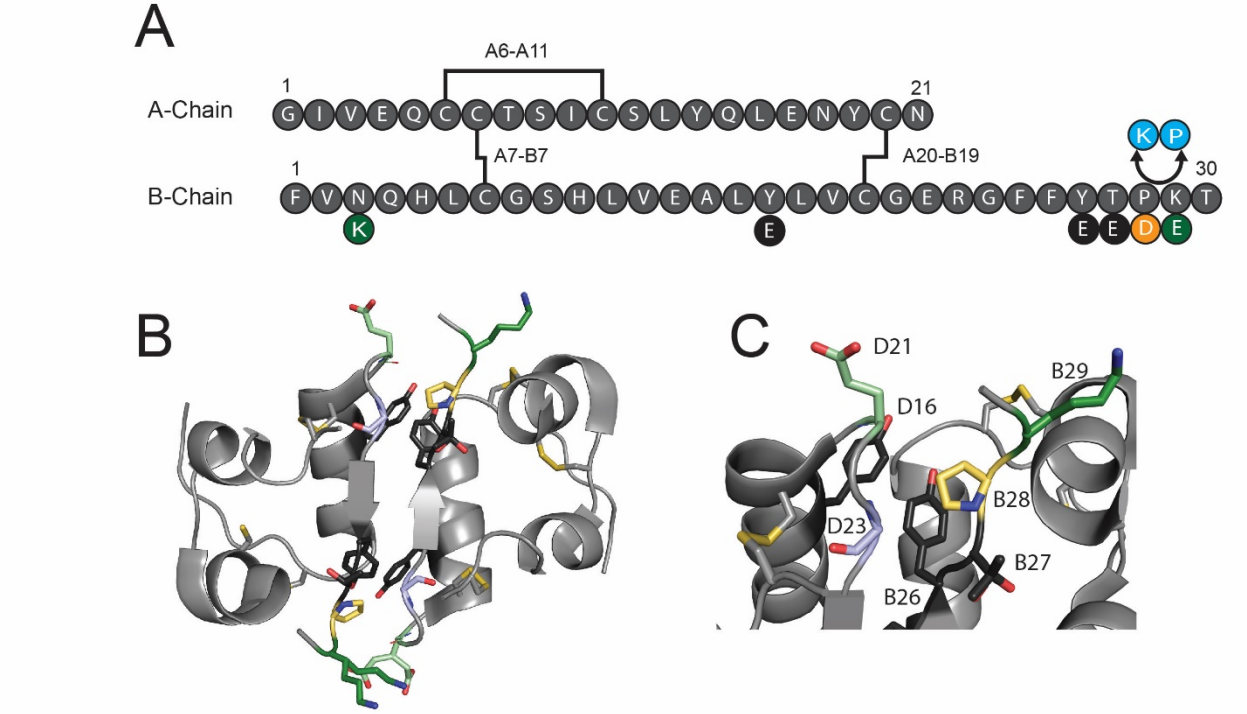

Figure S1. Structural summary of rapid-acting insulin analogs. (*A*) Representation of modifications to the sequence of insulin to create rapid-acting insulin analogs. Insulin lispro (developed by analogy to insulin-like growth factor-I [IGF-I]), highlighted the Pro^{B28}/Gly^{D23} dimer contact (highlighted in *sky blue* in panels *B* and *C*) (1). Other designs introduced polar or charged substitutions at the dimer interface. Among these were substitution of Thr^{B27}, Tyr^{B26}, or Tyr^{B16} by Glu (2,3) (shown as *black circles* in *A*). Clinical analogs insulin glulisine (Apidra®) and insulin aspart (Novolog®) contain acidic residues at positions B29 (*green*) and B28 (*yellow*), respectively (4). These residues were hypothesized to repel residue Glu^{D21}, impairing formation of dimers and higher-order oligomers (3). (*B*) The native residues of the positions listed above are highlighted in a 3D structure of an insulin dimer (PDB entry 5INS with color code as above). (*C*) Expanded view of panel *B* with residue positions as labeled.

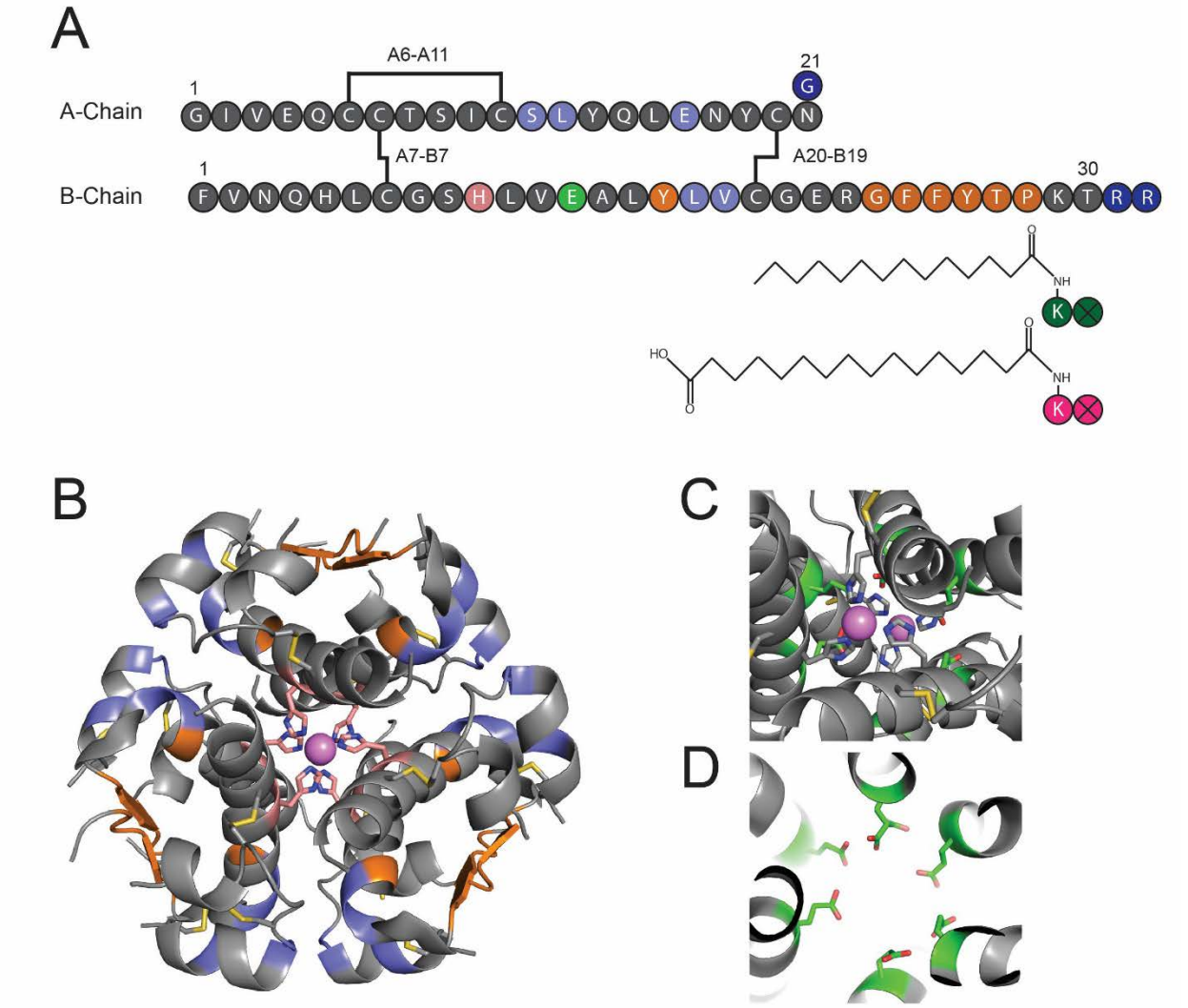

Figure S2. Past strategies to create basal insulin analogs (see also Table S10). (*A*) Sites in insulin modified in long-acting insulins. Insulin glargine (Lantus®; purple) represents the most successful product (5) with pI shifted towards neutrality due to a basic extension of the B chain. Such pI-shifted analogs are soluble as formulated at acidic but precipitate in the neutral environment of the SQ space to create a long-lived depot (6). A second class of basal insulins are derivatized with long acyl chains at Lys^{B29} (7). These include insulin detemir (Levemir®; *green circles*) and degludec (Tresiba®; *magenta circles*) (8), which bind to albumin as a "circulating depot (7)." Insulin degludec forms an acyl-linked dimer of zinc hexamers in its formulation but undergoes a switch to form an acyl-bridged, extended multihexameric linear complex in the SQ depot (8,9). These mechanisms are orthogonal to efforts to enhance the intrinsic stability of the insulin hexamer itself. Amino acid residues forming the dimer and hexamer interfaces of insulin in *orange* and *light blue*, respectively. His^{B10}, which coordinates with divalent zinc ions in hexamers, is highlighted in *pink*. (*B*) Dimer- and hexamer interfaces in the zinc insulin hexamer (T_6; color-coded as above). Analogs, designated "hydrophobic insulins," were engineered to contain hydrophobic substitutions at dimer or hexamer interfaces in an effort to stabilize the hexamer. Yet another class of analogs introduced hydrophobic substitutions to the surface of insulin hexamers to create non-specific multi-hexameric precipitates. However, the poor solubility of such analogs

limited their clinical utility (5). (*C*) Electrostatic stabilization of the insulin hexamer: view of the negatively charged ring formed by the six Glu^{B13} side chains (highlighted in *green*). An unobstructed view is shown in panel *D*. The most successful effort to stabilize the insulin hexamer involved substitution of Glu^{B13} by Gln, which eliminated repulsion within the Glu residues; however, the Gln^{B13} analog had reduced biological activity (3,10).

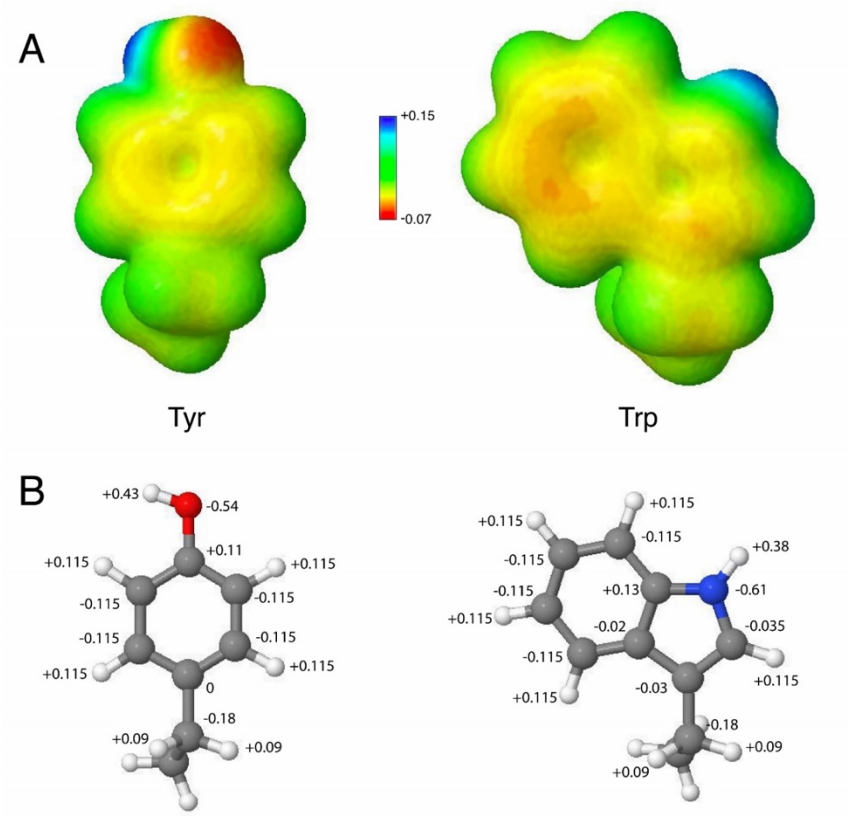

Figure S3. Comparison of *Ab initio* electrostatics and CHARMM parameters of Tyr and Trp side chains. (*A*) Isosurface representation of electron density and molecular electrostatic potential (MEP) map of Tyr (*left*) and Trp (*right*). Electron density and MEP were calculated using B3LYP method and 6-31G(d) basis set using Gaussian utility Cubegen on Gaussian 09 (11). The isosurface map was then generated using Jmol (12). (*B*) Ball-and-stick models of Tyr (*left*) and Trp (*right*) side chains. Point charges of each atom as implemented in CHARMM22 are indicated (13,14).

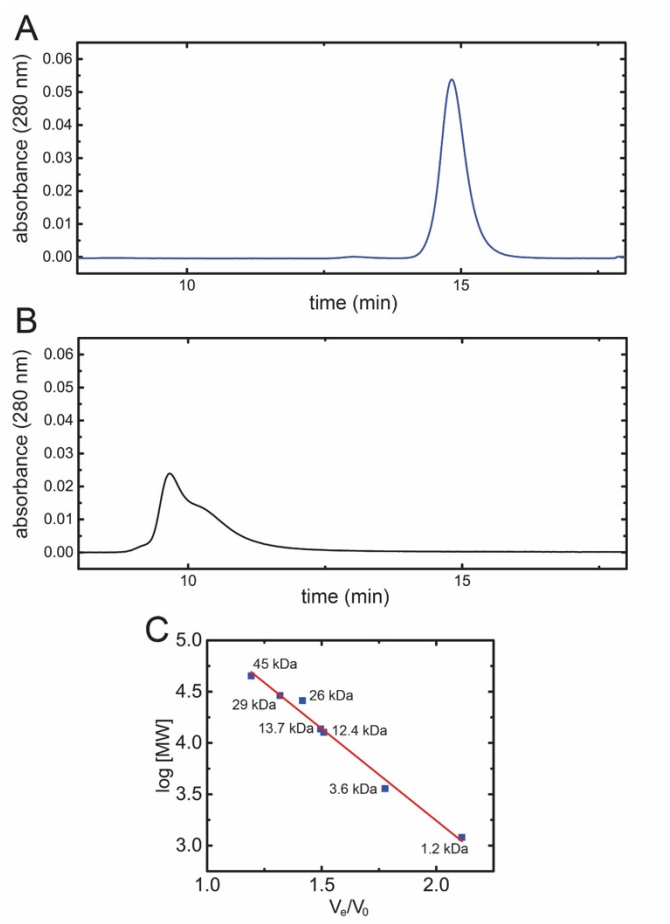

Figure S4. Solvent exclusion chromatography (SEC). Elution times of insulin in monomeric and hexameric states in SEC provide context for species identified in Figure 4. (*A*) SEC profile of monomeric lispro (Zn^{2+}-and phenol-free). The molecular weight (MW; or molecular mass) of the species was 3.1 kDa (calculated as in Fig. 4). (*B*) WT insulin formulated with 0.3 mM $ZnCl_2$ and phenol was run in a mobile-phase containing 50 mM cyclohexanol and 0.3 mM $ZnCl_2$. The sample eluted as a hexamer (Calculated molecular mass 48 kDa) with dissociation intermediates constituting the "tail" of the peak. (*C*) Calibration plot of SEC column with mobile phase used in panel *B*. Linear fit (*red line*) of log(MW) to V_e/V_0 of MW standards (*blue squares*). The equation of the line is log(MW) = -1.79 (V_e/V_0) +6.83 (R^2 = 0.986). The following standards were used for calibration: thyroglobulin (669 kDa, V_0), ovalbumin (45 kDa), carbonic anhydrase (29 kDa), elastase (26 kDa), ribonuclease A (13.7 kDa), cytochrome C (12.3 kDa) and synthetic peptides (3.6 and 1.2 kDa).

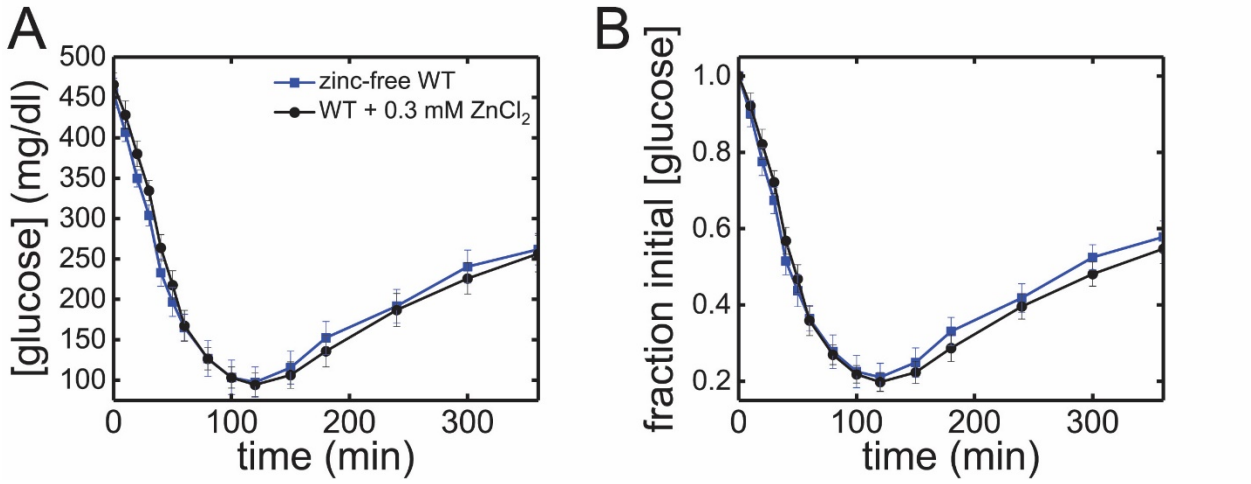

Figure S5. Effects of Zn^{2+} on PD profile of WT insulin. (*A*) Time course of [blood glucose] after SQ injection of WT insulin formulated in absence of Zn^{2+} (*blue*; N=8) or in presence of 0.3 mM $ZnCl_2$ (*black*; N=9). (*B*) Normalized curves from panel *A*.

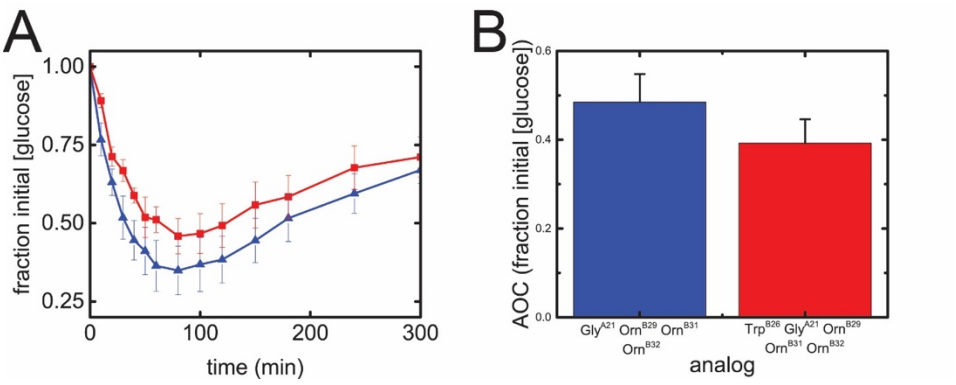

Figure S6. (*A*) Time course of [glucose] after IV injection of parent pI-shifted insulin analog (blue; N=6) and its Trp^{B26} derivative (red; N=6). (*B*) Bar graph showing area over curve (AOC) of curves from panel *A*. *Black bars* indicate S.E.M. The Trp^{B26} derivative displayed 82 ± 6% potency relative to the parent analog but is a complete agonist on injection of higher doses

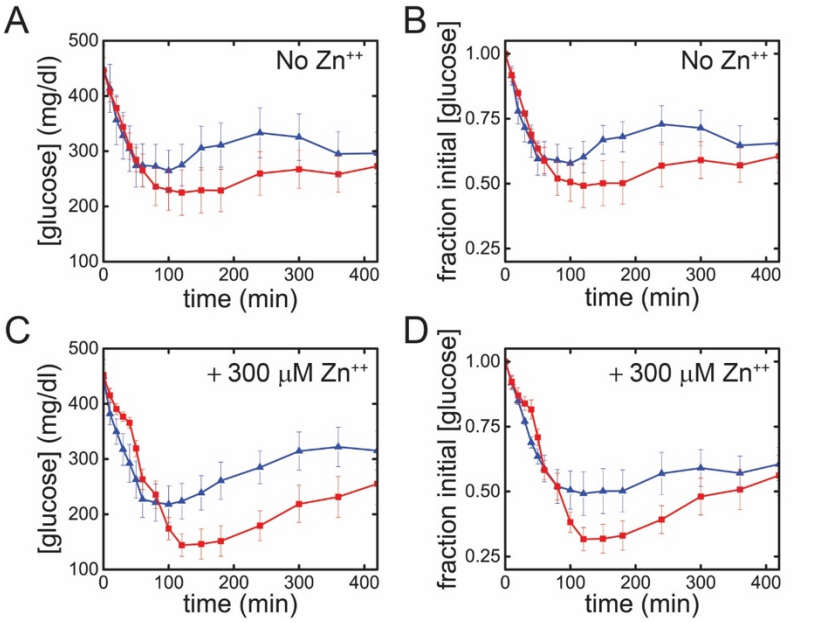

Figure S7. (*A*) Time course of [blood glucose] after SQ injection of zinc-free parent pI-shifted insulin analog (*blue*; N=6) and Trp^{B26} derivative (*red*; N=6). Normalized data are shown in *B*. (*C-D*) Corresponding plots of analogs administered after formulation in presence of 0.3 mM $ZnCl_2$, color-coded as above (N=6).

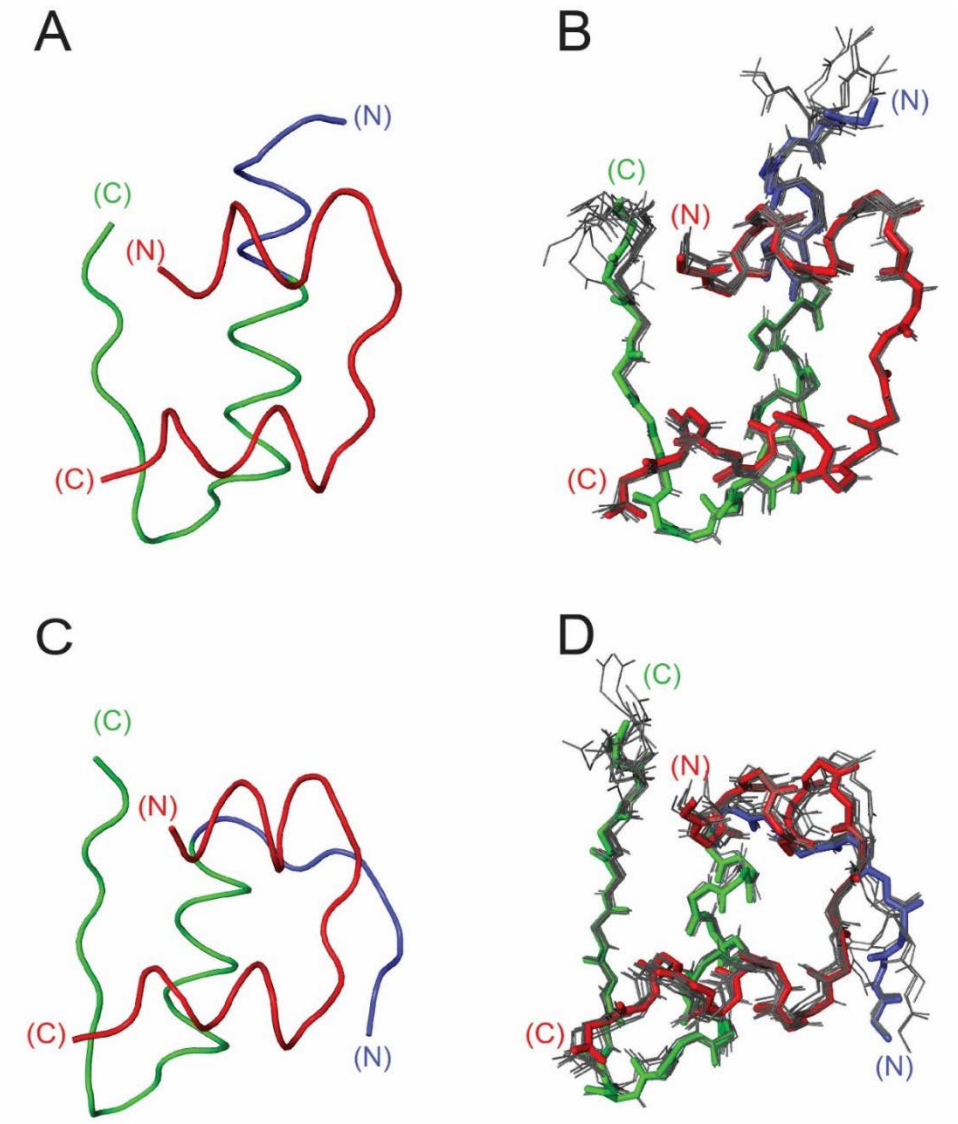

Figure S8. Comparison of the structure of Trp^{B26}, Orn^{B29}-insulin to a collection of WT insulin structures. (*A*) R^f-state protomer of Trp^{B26}, Orn^{B29}-insulin. The A chain is shown in *red*, and the B chain in *blue* (B1-B8) or *green* (B9-B30). (*B*) R^f-state protomer of Trp^{B26}, Orn^{B29}-insulin (*sticks*, color coded as above) in relation to extensive set of crystal structures of insulin and insulin analogs (PDB entries: 1BEN, 1G7A, 1RWE, 1EV3, 1EV6, 1MPJ, 1TRZ, 1TYL, 1MPJ, 1ZEG, 1ZNJ and 1ZNI; *gray sticks*). Structures are aligned with respect to the main-chain atoms of residues A1-A21 and B3- B28. RMSD values are given in Table S3. (*C-D*) Corresponding representations of the T-state protomer of Trp^{B26}, Orn^{B29}-insulin, color code as above. PDB entries used for alignment are as follows: 1APH, 1DPH, 1BEN, 1MPJ, 1TRZ, 1TYL, 1TYM, 1RWE, 1G7A, 1ZNI, 2INS and 4INS. RMSD values are given in Table S4.

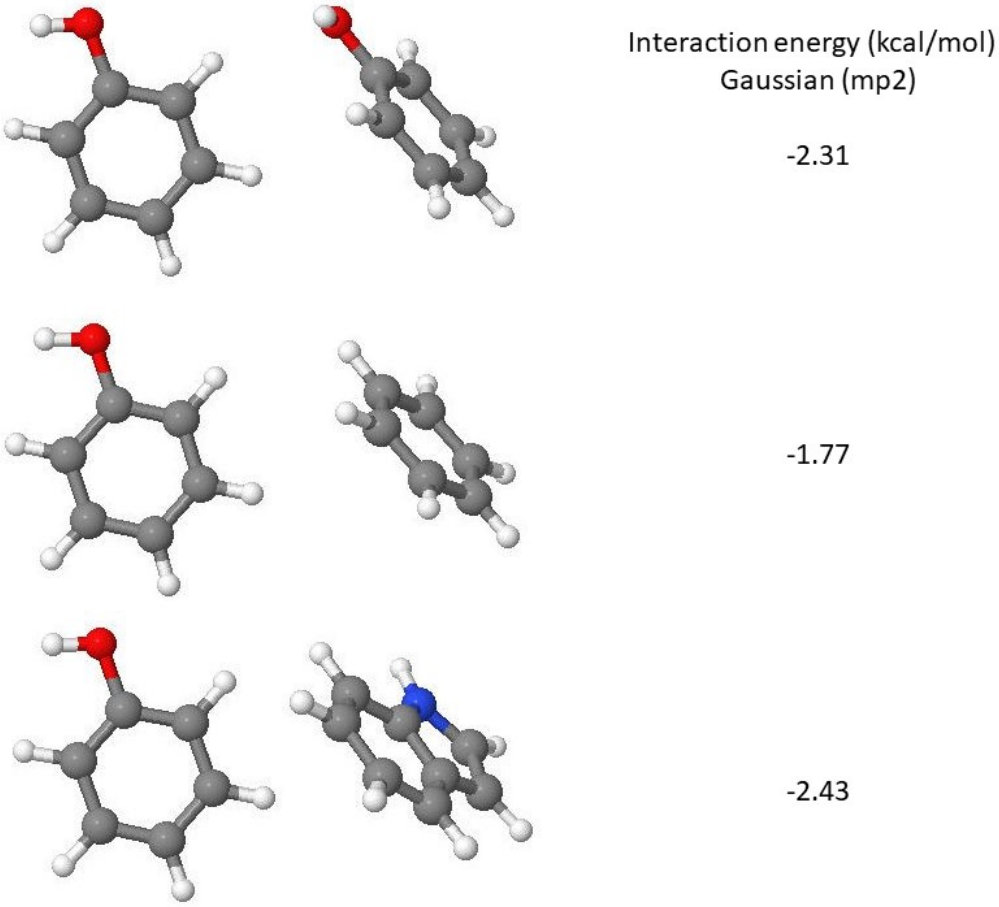

Figure S9. *Ab initio* calculations of energy of interaction between pairs of isolated aromatic molecules: phenol-phenol (*top*), phenol-benzene (*middle*), and phenol-indole (*bottom*). The phenol-indole pair was determined to form the most stable ETF interaction as a result of Van der Waals forces. Interaction energies were calculated using MP2 method and aug-cc-pVDZ basis set using Gaussian 09 (15).

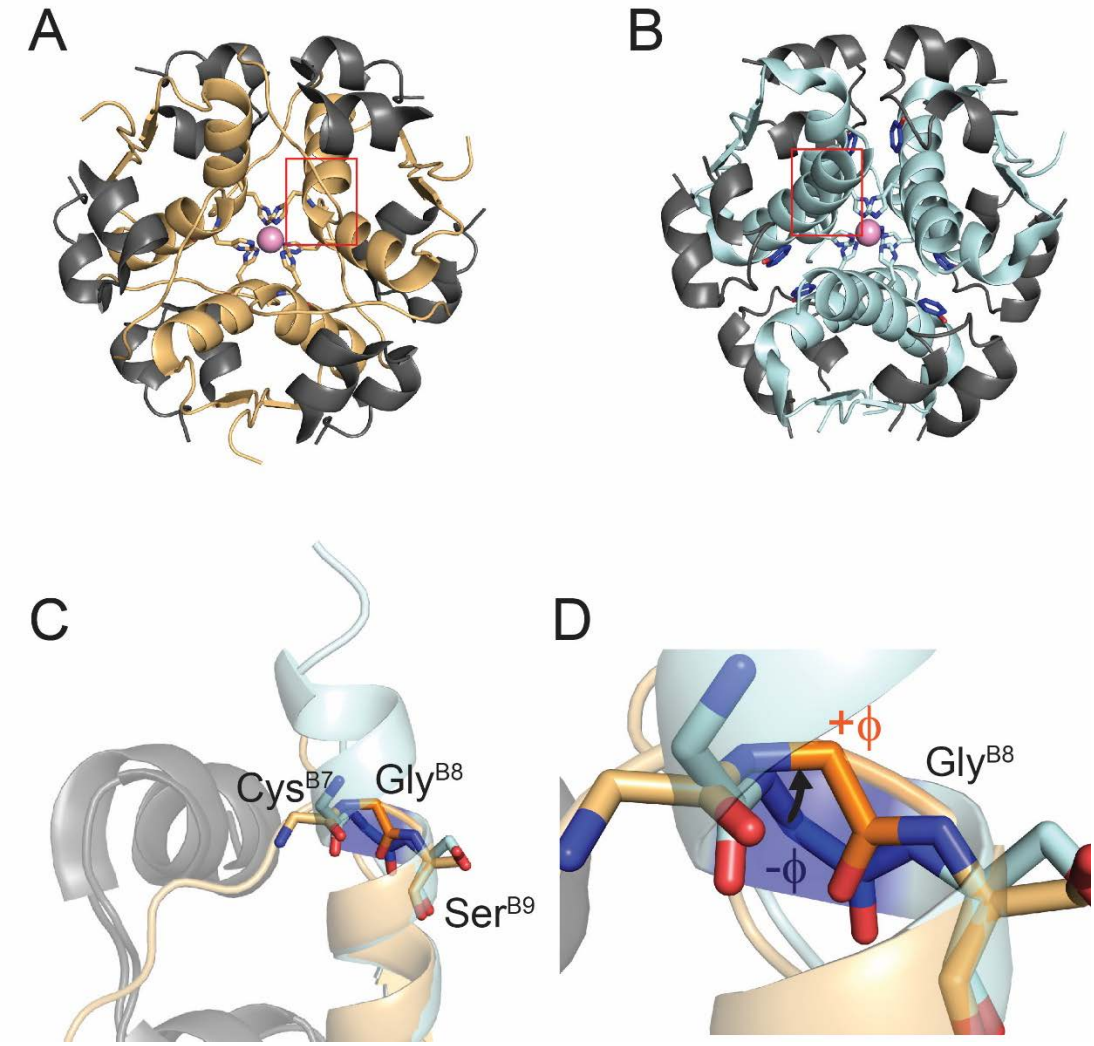

Figure S10. Structural representation of the classical T→R transition of the zinc insulin hexamer. (*A*) T_6 insulin hexamer. The eight N-terminal residues of the B chain (*orange*) are in an extended conformation (*red box*). (*B*) R_6 hexamer is stabilized by bound phenolic ligands (blue). Residues B1-B8 form an α-helix (*red box*). (*C*) Gly^{B8} serves as the pivot point of the transition between the R- (*blue*) and T-states (*orange*). (*D*) Gly^{B8} adopts a right-handed conformation (*i.e.*, with positive φ angle) in the T-state (*orange sticks*) and a left-handed conformation (negative φ angle) in the R-state (*blue sticks*).

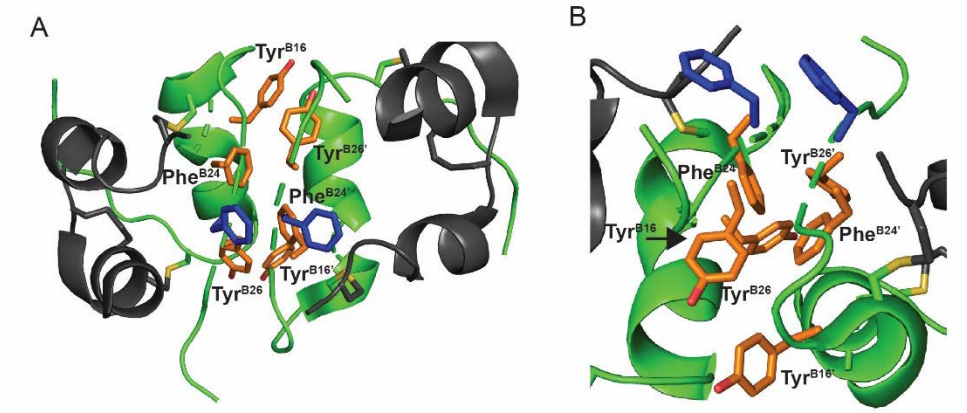

Figure S11. Ribbon model displaying the orientation of Phe^{B25} in the insulin dimer (PDB 4INS) in two views (*A, B*). The A chain is shown as dark gray ribbon, and the B chain is shown as *green ribbon*. Phe^{B25} (*blue sticks*) is peripheral to the aromatic network formed by Tyr^{B16}, Phe^{B24}, Tyr^{B26} and their symmetry-related mates (*orange sticks*).

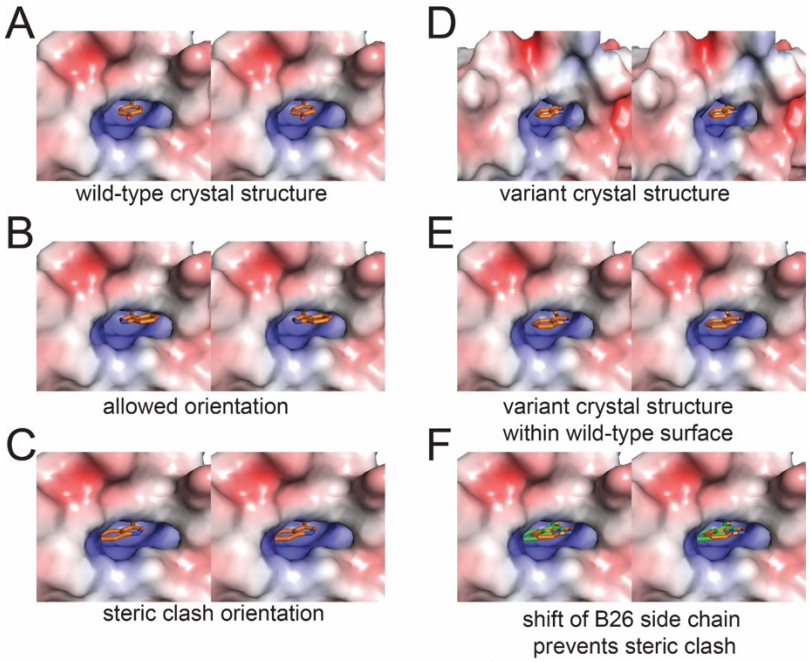

Figure S12. Comparison of B26 crevice within TR^{f} dimers of Trp^{B26}, Orn^{B29}-insulin to WT (1TRZ). (*A*) Stereo view of Tyr^{B26} (*sticks*) of 1TRZ T-state protomer within an electrostatic potential surface (generated using APBS plug-in to Pymol® (16)) formed by the surrounding residues (Fig. 1*D, E*). Positively-charged surfaces are represented in *blue*, negatively charged surfaces in *red*, and neutral surfaces in *white*. (*B, C*) Two possible orientations of the Trp^{B26} that retain χ_1 and χ_2 angles of the WT structure shown in panel *A*. Due to the asymmetric structure of the Trp side chain, two possible χ_2 angles of correspond in principle to the native Tyr. However, Trp^{B26} encounters a steric clash with residues in the core of insulin in the orientation shown in *C*. (*D*) Trp^{B26} of the R^{f}-state protomer from the Trp^{B26}, Orn^{B29}-insulin crystal structure depicted within an electrostatic potential surface formed by surrounding residues. (*E*) Depiction of Trp^{B26} from panel *D* within the B26 crevice from panel *A* (WT). The Trp^{B26} side chain does not encounter a steric clash. (*F*) Alignment of the naïve model of Trp^{B26} from panel *C* (*green sticks*) to the Trp^{B26},

Orn^{B29}-insulin structure (*orange sticks*). Residues are depicted within the WT crevice (*panels A, B, C,* and *E*). The steric clash predicted in the naïve model is mitigated in the Trp^{B26}, Orn^{B29}-insulin structure by (a) a local shift (0.2 Å) in the backbone of the C-terminal B-chain and (b) a slight difference in the χ_1 torsion angle of Trp^{B26}.

Table S1a. Interaction energy between the B26 residue of an energy minimized model of Trp^{B26} insulin relative to native Tyr^{B26} in the context of a TR^{f} dimer.

Residue	Interacting Residue	Total Energy of Interaction (kcal/mol)	
		1TRZ Tyr^{B26}	1TRZ Trp^{B26}
B26	Phe^{B24}	-0.344	-0.502
	Phe^{B25}	-0.100	-0.113
	Tyr^{B16}	-0.006	0.007
	Phe^{D24}	-0.887	-1.465
	Phe^{D25}	-0.029	-0.120
	Tyr/Trp^{D26}	0.000	-0.032
	Tyr^{D16}	-1.254	-1.672
D26	Phe^{B24}	-0.828	-1.436
	Phe^{B25}	0.005	-0.025
	Tyr/Trp^{B26}	0.000	-0.032
	Tyr^{B16}	-1.594	-0.503
	Phe^{D24}	-0.524	-0.699
	Phe^{D25}	-0.036	-0.084
	Tyr^{D16}	0.006	-0.005
Total		-6.986	-7.811

Table S1b. Local energy-minimized model of Trp^{B26} insulin relative to native Tyr^{B26} where polar atoms of Tyrosine and Tryptophan rings are replaced with nonpolar synthetic residues.

Residue	Interacting Residue	Total Energy of Interaction (kcal/mol)	
		1TRZ Tyo^{B26}	1TRZ Tro^{B26}
B26	Phe^{B24}	-0.358	-0.503
	Phe^{B25}	-0.090	-0.138
	Tyr^{B16}	0.006	0.009
	Phe^{D24}	-0.882	-1.501
	Phe^{D25}	-0.054	-0.095
	Tyr^{D26}	0.000	0.001
	Tyr^{D16}	-1.416	-1.527
D26	Phe^{B24}	-0.821	-1.478
	Phe^{B25}	0.005	-0.039
	Tyr^{B26}	0.000	-0.001
	Tyr^{B16}	-0.938	-0.209
	Phe^{D24}	-0.566	-0.708
	Phe^{D25}	-0.049	-0.061
	Tyr^{D16}	0.006	0.003
		-6.531	-7.438

[a] Tabulation of non-bonded interaction energy at the insulin dimer interface in the energy-minimized naïve model of Tyr^{B26}→Trp displays interactions most improved by the substitution.

[b] This table demonstrates the impact of π-π interactions on non-bonded interaction energy across the insulin dimer interface. Polar oxygen and nitrogen atoms are replaced, *in silico*, with non-polar synthetic atoms eliminating the confounding effects of polar interactions involving those atoms on free-energy calculations.

Table S1c. Interaction energy between the B26 residue of a local energy-minimized model of Trp^{B26} insulin relative to native Tyr^{B26} in the context of an R_2 dimer.

Residue	Interacting Residue	Total Energy of Interaction (kcal/mol)	
		1ZNJ Tyr^{B26}	1ZNJ Trp^{B26}
B26	Phe^{B24}	-0.501	-0.571
	Phe^{B25}	-0.142	-0.146
	Tyr^{B16}	0.008	0.008
	Phe^{D24}	-1.032	-1.308
	Phe^{D25}	-0.002	-0.027
	Tyr/Trp^{D26}	-0.011	-0.003
	Tyr^{D16}	-1.569	-1.996
D26	Phe^{B24}	-0.738	-1.283
	Phe^{B25}	0.004	-0.034
	Tyr/Trp^{B26}	-0.011	-0.003
	Tyr^{B16}	-0.613	-1.326
	Phe^{D24}	-0.683	-0.635
	Phe^{D25}	-0.120	-0.145
	Tyr^{D16}	0.004	0.008
Total		-5.406	-7.461

Table S1d. Interaction energy between the B26 residue of a local energy-minimized model of Trp^{B26} insulin relative to native Tyr^{B26} in the context of an T_2 dimer.

Residue	Interacting Residue	Total Energy of Interaction (kcal/mol)	
		4INS Tyr^{B26}	4INS Trp^{B26}
B26	Phe^{B24}	-0.397	-0.549
	Phe^{B25}	-0.027	-0.058
	Tyr^{B16}	0.003	0.006
	Phe^{D24}	-1.405	-1.181
	Phe^{D25}	-0.008	-0.017
	Tyr/Trp^{D26}	-0.008	-0.054
	Tyr^{D16}	-1.643	-1.868
D26	Phe^{B24}	-1.242	-0.679
	Phe^{B25}	-0.016	-0.022
	Tyr/Trp^{B26}	-0.016	-0.054
	Tyr^{B16}	-2.710	-1.261
	Phe^{D24}	-0.365	-0.466
	Phe^{D25}	-0.049	-0.140
	Tyr^{D16}	0.004	0.006
Total		-7.879	-6.337

Table S2. Data collection and refinement statistics pertaining to the crystal structure of Trp^{B26}, Orn^{B29}-insulin.

Data Collection	
Source	SSRL BL7-1
wavelength (Å)	0.9795
space group	R3
Unit-cell dimensions	a = 79.7552 Å, b = 79.7552 Å, c = 37.61 Å, α = 90°, β = 90°, γ = 120°
resolution (Å)	33.04-2.25
R_{merge} (%)	3.698 (10.28)
$I/\sigma I$	45.78 (8.99)
completeness (%)	99.5 (99.8)
redundancy	10.1 (9.6)
no. of reflections/used in refinement	4273/4226
Refinement	
resolution (Å)	33.04-2.25
R-factor/R_{Free} (%)	16.8/24.9
r.m.s.d. bond length (Å)	0.036
r.m.s.d. bond angle (°)	.971
median B-factors ($Å^2$)	
chain A	28
chain B	22
chain C	27
chain D	18
Ramachandran plot (%)	
most favored region	100
additionally allowed regions	0
generously allowed regions	0
disallowed regions	0

Table S3. RMSD values of main-chain and side-chains of the R-state protomer in the crystal structures of Trp^{B26}, Orn^{B29}-insulin and selected WT R_6 and T_3R_3 hexamers.

PDB ID	main-chain RMSD (Å)	Side-chain RMSD (Å)
1RWE R^f $(T_3R_3)^a$	0.70	1.25
1BEN R^f (T_3R_3)	0.39	0.97
1TRZ R^f (T_3R_3)	0.43	0.95
1TYL R^f (T_3R_3)	0.46	1.04
1TYM R^f (T_3R_3)	0.44	1.10
1ZNI R^f (T_3R_3)	0.45	0.89
1MPJ R^f (T_3R_3)	0.45	0.91
3MTH R^f (T_3R_3)	0.52	1.18
1LPH R^f (T_3R_3)	0.53	1.07
1G7A $R1^f$ (rhom T_3R_3)	0.61	1.06
$R2^f$	0.79	1.53
1EV3 R1 (rhom R_6)^b	0.71	1.59
R2	0.56	1.32
1ZEG R1 (rhom R_6)	0.52	1.35
R2	0.61	1.82
1ZEH R1 (rhom R_6)	0.55	1.25
R2	0.66	1.85
1ZNJ R1 (monoclinic R_6)^c	0.62	1.37
R2	0.56	1.66
R3	0.76	1.79
R4	0.61	1.18
R5	0.63	1.47
R6	0.66	1.23

Continued on next page

1EV6 R1 (monoclinic R_6)[b]	0.68	1.53
R2	0.58	1.56
R3	0.82	1.94
R4	0.59	1.27
R5	0.65	1.83
R6	0.58	1.54
Average	0.59 ± 0.11	1.36 ± 0.30

[a] R^f or "R-frayed" indicates that the first three residues of the insulin B chain (B1-B3) are in a coil conformation rather than part of the B1-B16 helix, as in standard R-state structures.

[b] Rhombohedral crystals contain two unique R-state protomers in the asymmetrical unit that are related by 3-fold symmetry to the two other R-state dimers comprising an R_6 hexamer.

[c] Monoclinic R_6 crystals contain 6 individual R-state protomers in the asymmetrical unit.

Table S4. RMSD values of main-chain and side-chains of the T-state protomer of the crystal structures of Trp^{B26}, Orn^{B29}-insulin and selected WT T_6 and T_3R_3 hexamers

PDB ID	Main-chain RMSD (Å)	side-chain RMSD (Å)
1RWE T (T_3R_3)	0.302	1.18
1BEN T (T_3R_3)	0.289	0.67
1TRZ T (T_3R_3)	0.316	1.09
1TYL T (T_3R_3)	0.319	1.38
1TYM T (T_3R_3)	0.295	1.07
1ZNI T (T_3R_3)	0.283	0.68
1MPJ T (T_3R_3)	0.382	0.84
3MTH T (T_3R_3)	0.318	0.94
1LPH T (KP T_3R_3)	0.486	0.95
1G7A T1 (rhom T_3R_3)[a]	0.307	0.75
T2	0.334	1.16
4INS T1 (2ZN T_6)	1.127	1.94
T2	0.686	1.49
1APH (cubic T_2)[b]	0.620	1.00
1BPH (cubic T_2)	0.653	1.12
1CPH (cubic T_2)	0.667	1.32
1DPH (cubic T_2)	0.659	1.21
Average	0.47 ± 0.11	1.11 ± 0.30

[a] Rhombohedral crystals contain two unique T-state protomers in the asymmetrical unit that are related by 3-fold symmetry to the two other TR dimers comprising an T_3R_3 hexamer.

[b] Cubic T_2 crystals contain two T-state protomers forming an insulin dimer. They are zinc-free crystals.

Table S5. Comparison of χ_1 and χ_2 dihedral-angle values of the T protomer of the Trp^{B26}, Orn^{B29}-insulin crystal structure to the B26 side chains of WT T_6 or T_3R_3 insulin crystal structures[a]

PDB ID	chain	χ_1	χ_2
Trp^{B26}, Orn^{B29}-insulin	B	167.131	-108.457
1TRZ	B	-179.531	78.679[b]
4INS	B	170.768	66.198
	D	175.602	-113.722
2INS	B	170.867	63.894
	D	170.708	-111.824
1ZNI	D	178.670	67.486
1BEN	B	178.543	67.578
	D	172.629	60.183
3MTH	D	178.321	70.378

[a] Tabulation of χ_1 and χ_2 angles demonstrates the native-like orientation of the Trp^{B26} ring of the T protomomer of the Trp^{B26}, Orn^{B29}-insulin crystal structure.
[b] Due to the symmetric structure of the Tyr side chain, χ_2 and χ_2-180° are equivalent. For example, 78.679° is equivalent to -101.321°.

Table S6. Comparison of χ_1 and χ_2 dihedral angle values of the R protomomer of Trp^{B26}, Orn^{B29}-insulin crystal structure to the B26 side chains of WT R_6 or R^f insulin crystal structures[a]

PDB ID	chain	χ_1	χ_2
WB26	D	-179.108	-102.751
1TRZ	D	179.520	81.505[b]
1ZNJ	B	-173.898	82.727
	D	168.865	-90.454
	F	-176.674	69.837
	H	176.540	74.677
	J	-173.848	80.139
	L	175.389	72.440
	B	-178.950	77.319
1BEN	D	-162.232	84.877
1MPJ	B	-177.306	-89.456
3MTH	B	-173.822	-87.442

[a] Tabulation of χ_1 and χ_2 angles demonstrates the native-like orientation of the Trp^{B26} ring of the R protomomer of the Trp^{B26}, Orn^{B29}-insulin crystal structure.

[b] Due to the symmetric structure of the Tyr side chain, χ_2 and χ_2-180° are equivalent.

Table S7. Comparison of predicted proton-proton distances involving Trp^{B26} from Trp^{B26}, Orn^{B29}-insulin crystal structure and Trp^{B26}-associated NOEs in Trp^{B26} lispro

Trp Proton	Residue	Proton	Predicted Distance[a] (Å)	NOE Strength[b]
H-ε3	Ile^{A2}	H-δ1	3.82	w
H-ζ3	Val^{B12}	H-γ1[c]	6.93	s
H-ζ3	Val^{B12}	H-γ2	4.61	s
H-η2	Val^{B12}	H-γ1	7.61	m
H-η2	Val^{B12}	H-γ2	4.68	m
H-ζ2	Val^{B12}	H-γ1	7.38	w
H-ζ2	Val^{B12}	H-γ2	4.40	w
H-ε3	Val^{B12}	H-γ1	8.85	w
H-ε3	Val^{B12}	H-γ2	4.24	w
H-ε3	Leu^{B15}	H-δ1	3.24	w
H-ε3	Leu^{B15}	H-δ2	6.04	w
H-ζ3	Leu^{B15}	H-δ1	4.74	w
H-ζ3	Leu^{B15}	H-δ2	6.85	w

[a] Predicted distances were obtained from the AB (T-state) protomer of the Trp^{B26}, Orn^{B29}-insulin crystal structure.
[b] NOEs were categorized as strong (s, <4.0 Å), medium (m, 4.4-5.5 Å), and weak (w, >5.5 Å).
[c] Predicted proton-proton distances are provided for protons at equivalent carbon positions although associated NOEs are difficult to differentiate.

Table S8. Comparison of predicted proton-proton distances involving Tyr^{B26} from WT crystal structure and Tyr^{B26}-associated NOEs from lispro NMR spectrum.

Tyr Proton	Residue	Proton	Predicted Distance[a] (Å)	NOE Strength[b]
H-ε	Ile^{A2}	H-δ1	5.17	w
H-ε	Val^{A3}	H-γ1[c]	6.82	w
H-ε	Val^{A3}	H-γ2	4.05	w
H-δ	Val^{A3}	H-γ1	4.12	w
H-δ	Val^{A3}	H-γ2	6.25	w
H-ε	Leu^{B11}	H-β	4.61	w
H-ε	Leu^{B11}	H-γ	3.13	w
H-ε	Leu^{B11}	H-δ1	5.42	w
H-ε	Leu^{B11}	H-δ2	3.67	w
H-δ	Leu^{B11}	H-δ1	5.75	w
H-δ	Leu^{B11}	H-δ2	5.24	w
H-ε	Val^{B12}	H-γ1	7.21	w
H-ε	Val^{B12}	H-γ2	4.72	w
H-ε	Leu^{B15}	H-δ1	5.12	w
H-ε	Leu^{B15}	H-δ2	7.80	w
H-δ	Leu^{B15}	H-δ1	3.14	m
H-δ	Leu^{B15}	H-δ2	6.14	w
H-δ	Phe^{B24}	H-ε	4.55	w
H-δ	Thr^{B27}	H-γ2	6.88	w

[a] Predicted distances were obtained from the AB (T-state) protomer of WT structure 1TRZ.
[b] NOEs were categorized as strong (s, <4.0 Å), medium (m, 4.4-5.5 Å) or weak (w, >5.5 Å).
[c] Predicted proton-proton distances are provided for protons at equivalent carbon positions although associated NOEs are difficult to differentiate.

Table S9a. Energy of non-bonded interaction of Tyr^{B26} with local aromatic residues[a]

Protomer	Residue	Interaction Energy (kcal/mol)
Tyr^{B26}	B24F	-0.323
	B25F	-0.111
	B16Y	0.007
	D24F	-1.010
	D25F	-0.014
	D26Y	0.000
	D16Y	-1.310
Tyr^{D26}	B24F	-1.063
	B25F	0.001
	B26Y	0.000
	B16Y	-1.391
	D24F	-0.443
	D25F	-0.033
	D16Y	0.006
Total		-7.252

[a] As calculated from WT structure 1TRZ.

Table S9b. Energy of non-bonded interaction of Trp^{B26} with neighboring aromatic residues[a]

Protomer	Residue	Interaction Energy (kcal/mol)
Trp^{B26}	B24F	-0.375
	B25F	-0.162
	B16Y	0.009
	D24F	-1.266
	D25F	-0.023
	D26Y	0.015
	D16Y	-1.411
Trp^{D26}	B24F	-1.517
	B25F	-0.013
	B26Y	0.015
	B16Y	-2.073
	D24F	-0.733
	D25F	-0.073
	D16Y	0.007
Total		-8.670

[a] Table (calculated from Trp^{B26} Orn^{B29} structure) show specific aromatic-aromatic aromatic interactions improved in the TR dimer of Trp^{B26} Orn^{B29}-insulin in relation to WT insulin.

Table S10. Summary of previous designs of basal insulin analogs[a]

Modification	Mechanism	Drawbacks
Human Proinsulin	C-peptide slows absorption, prolongs activity (17)	Safety concerns regarding hyperproinsulinemia and cardiovascular side effects Not a truly basal insulin (17)
Neutral Protamine Hagedorn / Neutral Protamine Lispro	Forms crystals with partner molecule protamine (18)	Consistent dosing difficult (19) Intermediate acting (20) Can cause allergic reactions (21)
Gln^{B13}	Forms zinc-free hexamers (10)	Dramatically reduced biological activity (5)
Lys^{B27}	Positive charge of stabilizes packing of multiple hexamers (22) Shifts pI of insulin	Effective only in complement with other modifications (22)
Gln^{B13} Gln^{A17} Lys^{B30}	Iso-electric precipitation Stabilization of Hexamer	Dramatically reduced biological activity (23)
Gly^{A21},Arg^{B27},Thr^{B30}-NH2	Iso-electric precipitation in subcutaneous depot, Gly^{A21} prevents chemical degradation in acidic formulations (23)	Macrophage invasion and inflammation at injection site (7,24)
Gly^{A21} $Arg^{B30}Arg^{B31}$	Iso-electric precipitation in subcutaneous depot, Gly^{A21} prevents chemical degradation in acidic formulations	Reports of association with neoplasms (25) PK/PD profile less predictable than other basal analogs (26) Unknown effect of enzymatic degradation products (25,27)
Myristic acid-coupled Lys^{B29}	Slows absorption from SubQ depot, binds to albumin (24)	Reduced potency (24)
Hexadodecandioic acid-coupled Lys^{B29}	Slows absorption from SubQ depot, forms multihexameric complexes, binds to albumin (8,28)	Reduced potency, has not yet been used long-term clinically(8)

[a] This table underscores the challenges associated with the development of insulin analogs with protracted PD profiles. Trp^{B26} insulin analogs are unique in their ability to protract the PD profile of insulin by stabilizing the hexamer without significantly compromising the potency of the analog.

Table S11a. Intercentroid distances and angles between Tyr^{B26} and local aromatic residues[a]

	B26		D26	
Residue	r	Dih.A	r	Dih.A
B16	13.6	76	6.0	52
B24	7.3	85	5.9	87
B25	10.9	34	10.6	70
B26	-	-	12.0	77
D16	5.8	58	13.1	89
D24	5.8	38	7.5	78
D25	12.6	38	9.5	45
D26	12.0	77	-	-

Table S11b. Intercentroid distances and angles between Tyr^{B26} and local aromatic residues[a]

	B26		D26	
Residue	r	Dih.A	r	Dih.A
B16	12.8	90	5.5	20
B24	7.8	79	5.9	25
B25	9.7	37	13.0	44
B26	-	-	12.2	73
D16	5.6	51	13.7	66
D24	6.6	46	7.0	89
D25	10.9	73	11.1	10
D26	12.2	73	-	-

[a] Tables S11a and S11b (respectively calculated from WT structure 1TRZ and the present crystal structure of the TrpB26 analog) indicate the character of aromatic-aromatic interactions involving Tyr or Trp^{B26} at the insulin dimer interface. Whereas some interactions are classical ETF interactions, others show some deviation in ring-to-ring dihedral angle (Dih.A).

Table S12a. Thermodynamic stabilization associated with the B26 side chain during folding of insulin analogs[a]

Side Chain	ΔSA	ΔG_u [b] (kcal/mol)	Side Chain	ΔSA	ΔG_u (kcal/mol)
Tyr^{B26}	68.9%	0.49 [a]	Trp^{B26}	69.3%	1.4
Tyr^{D26}	78.6%	0.56	Trp^{D26}	70.1%	1.5
Mean $\Delta\Delta G_u$: 0.9 kcal/mol (not observed)					

Table S12b. Thermodynamic stabilization associated with the B26 side chain during dimerization of insulin analogs[a]

Side Chain	ΔSA	ΔG_u (kcal/mol)	Side Chain	ΔSA	ΔG_u (kcal/mol)
Tyr^{B26}	25.9%	0.18	Trp^{B26}	26.6%	0.55
Tyr^{D26}	78.6%	0.56	Trp^{D26}	26.5%	0.55
Mean $\Delta\Delta G_u$: 0.37 + 0.42 = 0.8 kcal/mol/dimer interface					

[a] The relative thermodynamic stabilities of Tyr^{B26} and Trp^{B26} insulin monomers calculated using hydrophobic transfer free energies contrasted with those determined by guanidine-denaturation assays. However, NMR data suggests dimerization may be favored in Trp^{B26} lispro to a greater extent than in native lispro.

[b] Tabulated values of respective H_2O/octanol transfer free energies are -0.71 kcal/mol (Tyr) and -2.09 kcal/mol (Trp) as described (29). This calculation pertains only to changes in exposure of residue B26 and does not consider secondary changes in exposure of neighboring side chains.

Table S13. Native-like crystal structures of R_6 hexamers formed by mutant insulin.

PDB ID or Reference	Modification
1EV6	WT Human Insulin
1ZNJ	Porcine insulin: Ala^{B30} at chain terminus
4E7V	Bovine Insulin: Ala^{A8}, Val^{A10}, Ala^{B30} at surfaces
3GKY	His^{A8}, Val^{A16} at surface (A8) or in core (A16)
4P65	Cha^{B24} at dimer interface
3ROV	D-Ala^{B20}, D-Ala^{B23}, lispro within β-turn
5HRQ	cis-hydroxyproline^{B28} at edge of dimer interface
5HPU	trans-hydroxyproline^{B28} at edge of dimer interface
5URU	Dihydroxyproline^{B28} at edge of dimer interface
5UQA	4-fluoro-proline^{B28} at edge of dimer interface
2WS6	N-methyl-Tyr^{B26} at dimer interface and inter-chain
2WS7	Pro^{B26} at dimer interface
3ZS2	Tyr^{B25}, N-methyl-Phe^{B26}, lispro at dimer interface
3ZQR	N-methyl-Phe^{B25} at dimer interface
5EMS	3-iodotyrosine^{B26}, Norleucine^{B29} at dimer interface
1QIY	Tyr^{B5} at inter-chain crevice
1ZEG	Asp^{B28} at edge of dimer interface
3ZU1	*Des*-B30, Nε-ω-carboxyheptadecanoyl-Lys^{B29}
Derewenda, 1987 (30)	$Val^{B12} \rightarrow$ Ile at dimer interface

Supplemental References:

1. Holleman, F., and Hoekstra, J. B. (1997) Insulin lispro. *N. Engl. J. Med.* **337**, 176-183
2. Brange, J., Ribel, U., Hansen, J. F., Dodson, G., Hansen, M. T., Havelund, S., Melberg, S. G., Norris, F., Norris, K., and Snel, L. (1988) Monomeric insulins obtained by protein engineering and their medical implications. *Nature* **333**, 679-682
3. Brange, J., and Vølund, A. (1999) Insulin analogs with improved pharmacokinetic profiles. *Adv. Drug Deliv. Rev.* **35**, 307-335
4. van Bon, A. C., Bode, B. W., Sert-Langeron, C., DeVries, J. H., and Charpentier, G. (2011) Insulin glulisine compared to insulin aspart and to insulin lispro administered by continuous subcutaneous insulin infusion in patients with type 1 diabetes: a randomized controlled trial. *Diabetes Technol. Ther.* **13**, 607-614
5. Markussen, J. M., Hougaard, P., Ribel, U., Sørensen, A. R., and Sørensen, E. (1987) Soluble, prolonged-acting insulin derivatives. I. Degree of protraction and crystallizability of insulins substituted in the termini of the B-chain. *Protein Eng.* **1**, 205-213
6. Gillies, P. S., Figgitt, D. P., and Lamb, H. M. (2000) Insulin glargine. *Drugs* **59**, 253-260
7. Markussen, J., Havelund, S., Kurtzhals, P., Andersen, A., Halstrøm, J., Hasselager, E., Larsen, U., Ribel, U., Schäffer, L., and Vad, K. (1996) Soluble, fatty acid acylated insulins bind to albumin and show protracted action in pigs. *Diabetologia* **39**, 281-288
8. Gough, S., Harris, S., Woo, V., and Davies, M. (2013) Insulin degludec: overview of a novel ultra long-acting basal insulin. *Diab. Obes. Metab.* **15**, 301-309
9. Steensgaard, D. B., Schluckebier, G., Strauss, H. M., Norrman, M., Thomsen, J. K., Friderichsen, A. V., Havelund, S., and Jonassen, I. (2013) Ligand-controlled assembly of hexamers, dihexamers, and linear multihexamer structures by the engineered acylated insulin degludec. *Biochemistry* **52**, 295-309
10. Bentley, G. A., Brange, J., Derewenda, Z., Dodson, E. J., Dodson, G. G., Markussen, J., Wilkinson, A. J., Wollmer, A., and Xiao, B. (1992) Role of B13 Glu in insulin assembly. The hexamer structure of recombinant mutant (B13 Glu→Gln) insulin. *J. Mol. Biol.* **228**, 1163-1176
11. Frisch, M. J., Trucks, G. W., Schlegal, H. B., Scuseria, G. E., Robb, M. A., Cheeseman, J. R., Scalmani, G., Barone, V., Mennucci, B., Petersson, G. A., Nakatsuji, H., Caricato, M., Li, X., Hratchian, H. P., Izmaylov, A. F., Bloino, J., Zheng, G., Sonnenberg, J. L., Hada, M., Ehara, M., Toyota, K., Fukuda, R., Hasegawa, J., Ishida, M., Nakajima, T., Honda, Y., Kitao, O., Nakai, H., Vrenven, T., Montogomery, J. A., Peralta, J. E., Ogliaro, F., Bearpark, M., Heyd, J. J., Brothers, E., Kudin, K. N., Staroverov, V. N., Kobayashi, R., Normand, J., Raghavachari, K., Rendell, A., Burant, J. C., Iyengar, S. S., Tomasi, J., Cossi, M., Rega, N., Millam, J. M., Klene, M., Knox, J. E., Cross, J. B., Bakken, V., Adamo, C., Jaramillo, J., Gomperts, R., Stratmann, R. E., Yazyev, O., Austin, A. J., Cammi, R., Pomelli, C., Ochterski, J. W., Martin, R. L., Morokuma, K., Zakrzewski, V. G., Voth, G. A., Salvador, P., Dannenberg, J. J., Dapprich, S., Daniels, A. D., Farkas, Foresman, J. B., Ortiz, J. V., Cioslowski, J., and Fox, D. J. (2009) Gaussian09 Revision D.01. Gaussian Inc., Wallingford, CT
12. Willighagen, E., and Howard, M. (2007) Fast and Scriptable Molecular Graphics in Web Browsers without Java3D. in *Nature Precedings*
13. Brooks, B. R., Brooks, C. L., Mackerell, A. D., Nilsson, L., Petrella, R. J., Roux, B., Won, Y., Archontis, G., Bartels, C., Boresch, S., Caflisch, A., Caves, L., Cui, Q., Dinner, A. R., Feig, M., Fischer, S., Gao, J., Hodoscek, M., Im, W., Kuczera, K., Lazaridis, T., Ma, J., Ovchinnikov, V., Paci, E., Pastor, R. W., Post, C. B., Pu, J. Z., Schaefer, M., Tidor, B., Venable, R. M., Woodcock, H. L., Wu, X., Yang, W., York, D. M., and Karplus, M. (2009) CHARMM: The biomolecular simulation program. *J. Comput. Chem.* **30**, 1545-1614

14. MacKerell, A. D., Brooks, B., Brooks, C. L., Nilsson, L., Roux, B., Won, Y., and Karplus, M. (2002) CHARMM: The Energy Function and Its Parameterization. in *Encyclopedia of Computational Chemistry* (Schleyer, P. v. R. C., N. L. A. T. , Gasteiger, J., Kollman, P. A., Schaefer, H. F., III, Schreiner, P. R. S. ed.), John Wiley & Sons, Ltd, Chichester. pp 271-277

15. Frisch, M. J., Trucks, G. W., Schlegel, H. B., Scuseria, G. E., Robb, M. A., Cheeseman, J. R., Scalmani, G., Barone, V., Mennucci, B., Petersson, G. A., Nakatsuji, H., Caricato, M., Li, X., Hratchian, H. P., Izmaylov, A. F., Bloino, J., Zheng, G., Sonnenberg, J. L., Hada, M., Ehara, M., Toyota, K., Fukuda, R., Hasegawa, J., Ishida, M., Nakajima, T., Honda, Y., Kitao, O., Nakai, H., Vreven, T., Montgomery, J., J. A. , Peralta, J. E., Ogliaro, F., Bearpark, M., Heyd, J. J., Brothers, E., Kudin, K. N., Staroverov, V. N., Kobayashi, R., Normand, J., Raghavachari, K., Rendell, A., Burant, J. C., Iyengar, S. S., Tomasi, J., Cossi, M., Rega, N., Millam, J. M., Klene, M., Knox, J. E., Cross, J. B., Bakken, V., Adamo, C., Jaramillo, J., Gomperts, R., Stratmann, R. E., Yazyev, O., Austin, A. J., Cammi, R., Pomelli, C., Ochterski, J. W., Martin, R. L., Morokuma, K., Zakrzewski, V. G., Voth, G. A., Salvador, P., Dannenberg, J. J., Dapprich, S., Daniels, A. D., Farkas, O., Foresman, J. B., Ortiz, J. V., Cioslowski, J., and Fox, D. J. (2009) Gaussian 09, Revision A.02. in *Gaussian, Inc., Wallingford CT*, Revision A.02 Ed.
16. Baker, N. A., Sept, D., Joseph, S., Holst, M. J., and McCammon, J. A. (2001) Electrostatics of nanosystems: application to microtubules and the ribosome. *Proc. Nat. Acad. Sci.* **98**, 10037-10041
17. Galloway, J. A., Hooper, S. A., Spradlin, C. T., Howey, D. C., Frank, B. H., Bowsher, R. R., and Anderson, J. H. (1992) Biosynthetic human proinsulin. Review of chemistry, *in vitro* and *in vivo* receptor binding, animal and human pharmacology studies, and clinical trial experience. *Diab. Care* **15**, 666-692
18. Hagedorn, H., Jensen, B. N., Krarup, N., and Wodstrup, I. (1936) Protamine insulinate. *JAMA* **106**, 177-180
19. Lauritzen, T., Pramming, S., Gale, E., Deckert, T., and Binder, C. (1982) Absorption of isophane (NPH) insulin and its clinical implications. *Brit. Med. J.* **285**, 159-162
20. Owens, D. R., and Bolli, G. B. (2008) Beyond the era of NPH insulin—long-acting insulin analogs: chemistry, comparative pharmacology, and clinical application. *Diabetes Technol. Ther.* **10**, 333-349
21. Stewart, W. J., Mcsweeney, S. M., Kellett, M. A., Faxon, D. P., and Ryan, T. J. (1984) Increased risk of severe protamine reactions in NPH insulin-dependent diabetics undergoing cardiac catheterization. *Circulation* **70**, 788-792
22. Markussen, J., Diers, I., Engesgaard, A., Hansen, M. T., Hougaard, P., Langkjaer, L., Norris, K., Ribel, U., Sorensen, A. R., Sorensen, E., and et al. (1987) Soluble, prolonged-acting insulin derivatives. II. Degree of protraction and crystallizability of insulins substituted in positions A17, B8, B13, B27 and B30. *Protein Eng.* **1**, 215-223
23. Markussen, J., Diers, I., Hougaard, P., Langkjaer, L., Norris, K., Snel, L., Sørensen, A. R., Sørensen, E., and Voight, H. O. (1988) Soluble, prolonged-acting insulin derivatives. III. Degree of protraction, crystallizability and chemical stability of insulins substituted in positions A21, B13, B23, B27 and B30. *Protein Eng.* **2**, 157-166
24. Kurtzhals, P., Havelund, S., Jonassen, I., Kiehr, B., Larsen, U., Ribel, U., and Markussen, J. (1995) Albumin binding of insulins acylated with fatty acids: characterization of the ligand-protein interaction and correlation between binding affinity and timing of the insulin effect in vivo. *Biochem. J.* **312**, 725-731
25. Suissa, S., Azoulay, L., Dell'Aniello, S., Evans, M., Vora, J., and Pollak, M. (2011) Long-term effects of insulin glargine on the risk of breast cancer. *Diabetologia* **54**, 2254-2262
26. Yamamoto, C., Miyoshi, H., Fujiwara, Y., Kameda, R., Ichiyama, M., Nomoto, H., Kameda, H., Nakamura, A., and Atsumi, T. (2016) Degludec is superior to glargine in terms of daily glycemic variability in people with type 1 diabetes mellitus. *Endocr. J.* **63**, 53-60

27. Sommerfeld, M. R., Muller, G., Tschank, G., Seipke, G., Habermann, P., Kurrle, R., and Tennagels, N. (2010) *In vitro* metabolic and mitogenic signaling of insulin glargine and its metabolites. *PLoS One* **5**, e9540
28. Jonassen, I., Havelund, S., Hoeg-Jensen, T., Steensgaard, D. B., Wahlund, P. O., and Ribel, U. (2012) Design of the novel protraction mechanism of insulin degludec, an ultra-long-acting basal insulin. *Pharm. Res.* **29**, 2104-2114
29. Wimley, W. C., and White, S. H. (1996) Experimentally determined hydrophobicity scale for proteins at membrane interfaces. *Nat. Struct. Molec. Biol.* **3**, 842
30. Derewenda, U., Derewenda, Z., Dodson, G., and Brange, J. (1987) The Crystal-Structure of the B-12 Ile Human Insulin Prepared by Site-Directed Mutatgenesis. *Protein Eng.* ***222****, 425-433*